PUBLICAÇÕES

IFUSP/P-684

THE EFFECT OF α-TRANSFER POLARIZATION POTENTIAL IN THE $^{24}Mg + ^{16}O$ SYSTEM

R. Lichtenthäler Filho, A. Lépine-Szily,
A.C.C. Villari and O. Portezan Filho

Instituto de Física, Universidade de São Paulo

Dezembro/1987

THE EFFECT OF α-TRANSFER POLARIZATION POTENTIAL IN THE $^{24}Mg + ^{16}O$ SYSTEM

R. Lichtenthäler Filho, A. Lépine-Szily, A.C.C. Villari and O. Portezan Filho

Instituto de Física, Universidade de São Paulo
C.P. 20516, 01498 São Paulo, SP, Brasil

ABSTRACT

The effect of the dynamic α-transfer polarization potential on several channels of the system $^{24}Mg + ^{16}O$ has been calculated and compared to our experimental data and those of Paul and collaborators. The general agreement is good, indicating that the α-transfer coupling can have an important contribution to explain the back-angle anomalies observed in the elastic, inelastic and transfer channels.

---

*Work supported by FINEP and CNPq.

I. INTRODUCTION

The anomalous back-angle elastic scattering of nα-type nuclei ($^{16}O + ^{28}Si$, $^{16}O + ^{24}Mg$, $^{12}C + ^{28}Si$, $^{12}C + ^{24}Mg$, etc.) has attracted considerable attention in the last decade. The transfer reactions ($^{16}O, ^{12}C$) involving these systems also present anomalous back-angle behaviour, with strongly oscillating backward rise in angular distributions and very structured backward excitation functions[1,2].

A possible mechanism to explain the deviations from standard strong absorption behaviour could be the coupling between elastic channel and the α-transfer channels. A first attempt[3] to include this coupling has been applied to the $^{24}Mg + ^{12}C$ elastic scattering at 40 MeV. The coupling to the $^{24}Mg(^{12}C, ^{16}O)^{20}Ne$ reaction was described in the framework of Frahn's diffused formalism[4] and a good agreement with data was obtained. In order to explain the anomalous back-angle excitation function of the $^{28}Si(^{16}O, ^{16}O)^{28}Si$ elastic scattering, the transfer of two and three α-particles was described in a semi-classical treatment[5] of the interplay between transfer process and absorption. The general trend of data is consistent with the calculated energy dependence.

In a recent work of Hussein and collaborators[6], the coupling to α-transfer channel has been explicitly taken into account by the evaluation of a dynamic α-transfer polarization

potential (DTPP) for the process $^{16}O + ^{28}Si \rightarrow ^{12}C + ^{32}S \rightarrow ^{16}O + ^{28}Si$ and the back angle elastic scattering of $^{16}O + ^{28}Si$ have been reproduced with the polarization potential added to the E-18 optical potential.

The aim of this work is to evaluate the effect of the dynamic α-transfer polarization potential (DTPP) on all observed channels and compare with experimental data. We measured the angular distributions of the elastic, inelastic, α-stripping and α-pick-up channels for the $^{16}O + ^{24}Mg$ system at E_{CM} = 27.8 MeV. The DTPP, describing the coupling between the elastic and the α-stripping channel, was calculated and introduced into a DWBA code and its effect on the elastic, inelastic and transfer cross-sections was calculated. The general agreement between measured angular distributions and calculations is good, indicating that the α-transfer coupling can have an important contribution to explain the back-angle anomalies.

II. EXPERIMENTAL METHOD AND RESULTS

The angular distributions of elastic, inelastic and transfer reactions of the system $^{16}O + ^{24}Mg$ were measured using an ^{16}O beam accelerated to E_{LAB} = 46.5 MeV by the São Paulo Pelletron Accelerator. Targets of isotopically enriched ^{24}Mg were evaporated on ^{12}C backing. Three sets of ΔE-E telescopes

were used, the E detectors being standard Si surface barrier detectors and the ΔE detectors proportional gas counters. A thin layer of Bi was evaporated on the ^{12}C backings before the ^{24}Mg evaporation and the Rutherford scattering of ^{16}O on Bi provided a practical way to normalize the data. A monitor placed at 15^{o} with respect to the beam permitted us to calculate the ratio of ^{24}Mg to Bi target thicknesses to obtain absolute cross-sections for all measured processes. The energy resolution at all angles was sufficient to separate the elastic peak from inelastic peaks.

Paul and collaborators[2] have measured at the same energy the angular distributions for $^{24}Mg(^{16}O,^{16}O)^{24}Mg$ elastic scattering, the back-angle inelastic scattering and the transfer reactions $^{24}Mg(^{16}O,^{12}C)^{28}Si$ leading to the ground state and the first excited 2^{+} state in ^{28}Si. Our measurements had an angular range $\theta_{lab} = 20^{o}-70^{o}$, being impossible to measure the reactions at very forward angles, due to fusion products from $^{16}O+^{12}C$ and $^{16}O+^{16}O$ fusion reactions.

In Fig. 1 we present our elastic and inelastic angular distributions. In Fig. 2 we present our transfer reaction $^{24}Mg(^{16}O,^{12}C)^{28}Si$ g.s. and $^{24}Mg(^{16}O,^{12}C)^{28}Si$ (2^{+}, 1.78 MeV) angular distributions and on Fig. 3 we show our data on $^{24}Mg(^{16}O,^{20}Ne)^{20}Ne$, leading respectively to the ^{20}Ne ground state, one ^{20}Ne excited to the 2^{+}, 1.63 MeV state, both ^{20}Ne excited to the 2^{+} state, one ^{20}Ne excited to the 4^{+}, 4.25 MeV state.

Our elastic scattering and ($^{16}O, ^{12}C$) data agree well with the measurents of Paul[2] from $\theta_{CM} = 35^{o}$ to 55^{o}. From 55^{o} to 100^{o} our data are more precise and present more structures. The $^{24}Mg(^{16}O, ^{20}Ne)^{20}Ne$ g.s angular distribution shown in Fig. 3 presents strong oscillations and a symmetry around 90^{o}, with a strong minimum at 90^{o}. The reaction leading to one excited $^{20}Ne(2^{+})$ has a slight minimum at 90^{o} and the reaction leading to both excited $^{20}Ne(2^{+})$ nuclei, presents a modest maximum at 90^{o}.

III. ANALYSIS OF THE DATA

A) THE DYNAMIC α-TRANSFER POLARIZATION POTENTIAL (DTPP)

Hussein and collaborators[6] define the dynamic α-transfer polarization potential (DTPP), $V_{pol.}$, to be the potential which reproduces, to first order, the correction to the elastic scattering T matrix, arising from an explicit consideration of the transfer process $0 \to 1 \to 0$, namely:

$$\Delta T_{00}^{(1)}(\vec{k},\vec{k}') = \langle \varphi_0 ; \chi^{(-)}(\vec{k}_0') | H_{01} G_1^{(+)} H_{10} | \varphi_0 ; \chi_0^{(+)}(\vec{k}_0) \rangle \quad (1)$$

$$\equiv \langle \chi_0^{(-)}(\vec{k}_0') | V_{pol} | \chi_0^{(+)}(\vec{k}_0) \rangle \quad (2)$$

where $\chi^{(\pm)}$ are the waves distorted by the background strong

absorption interaction, φ_0 is the intrinsic ground state of the combined system, H_{01} and H_{10} are the appropriate transfer coupling interactions and $G_1^{(+)}$ is the unperturbed distorted Green-function describing the propagation in channel 1, in the presence of the strong absorption potential. The DTPP can be expanded in partial waves and from this non-local DTPP a trivially equivalent local potential is defined through

$$\bar{V}^{\ell}_{pol}(r)\, f^0_{\ell}(kr) \equiv \int_0^{\infty} dr'\, V^{\ell}_{pol}(r,r')\, f^0_{\ell}(kr') \qquad (3)$$

where $f^0_{\ell}(kr)$ is the distorted partial wave function.

One finds that using the no recoil (NR) and zero range (ZR) approximations and including a factor of 2 due to off-shell corrections[7], the trivially equivalent local potential $\bar{V}_{pol}$ can be written as:

$$\bar{V}^{\ell}_{pol}(r) = C_{\ell}(E)\, F(r) \qquad (4)$$

where $F(r)$ is the form factor of the α-transfer reaction and $C_{\ell}(E)$ is given by:

$$C_{\ell}(E) = A \left(- \frac{4i\mu_1}{\hbar^2 k_1} \frac{(I^{01}_{\ell}(k_0,k_1))^2}{I^{00}_{\ell}(k_0)\, S^{N}_{\ell,1}(k_1)} \right) \qquad (5)$$

where A contains the spectroscopic amplitudes, normalization

due to recoil and finite range effects, I_ℓ^{01} is the NR, ZR transfer radial integral, I_ℓ^{00} is the NR, ZR elastic radial integral and $S^N_{\ell,1}$ are the unperturbed nuclear elastic scattering matrix elements in the transfer channel.

B) APPLICATION TO THE SYSTEM $^{24}Mg + ^{16}O$ AT $E_{CM} \approx 27.8$ MeV

1. Details of the calculation:

We apply the formalism of DTPP to the system $^{24}Mg + ^{16}O$, assuming the α-transfer process $^{24}Mg + ^{16}O \rightarrow ^{28}Si + ^{12}C \rightarrow ^{24}Mg + ^{16}O$ as a basis for our coupled-channels discussion. The corresponding polarization potential is constructed with channel 0 being $^{24}Mg + ^{16}O$ and channel 1 being $^{28}Si + ^{12}C$ and all participating nuclei are in their respective ground states. We modified the DWBA code DWUCK, which uses the no-recoil (NR) and zero-range (ZR) approximations in order to calculate $\bar{V}_{pol}$ and the cross-sections.

The calculations were performed in the following steps:

a) The NR and ZR radial integrals I_ℓ^{01} and I_ℓ^{00} and the scattering matrix $S^N_{\ell,1}$ were calculated by the DWBA code DWUCK together with the α-transfer form factor F(r), computing subsequently the polarization potential $\bar{V}_{pol}$.

b) The overall normalization of the polarization potential

thus obtained includes spectroscopic factors, recoil and finite range effects. In order to estimate the effect of ZR and NR approximations, we compared the transfer differential cross-section calculated by DWUCK (without $\bar{V}_{pol}$) and by the full finite range DWBA code PTOLEMY[8] for the reaction $^{24}Mg(^{16}O,^{12}C)^{28}Si$ g.s, using the optical potential obtained by Tabor[9], called ANL2 (see Table I) in the incoming and outgoing channels. The bound-state wave functions are calculated in the usual way, adjusting the depth of a Woods-Saxon well with $R = 1.25\ A_T^{1/3}$ fm and $a = 0.65$ fm, in order to reproduce the separation energies. The transferred four-nucleon cluster (called an α-particle hereafter) is assumed to be in an internal 1S state. Both calculations give very similar angular distributions, as can be seen in Fig. 4, resulting in a constant normalization factor which takes into account the recoil and finite range effects. The full normalization of $\bar{V}_{pol}$, including also spectroscopic factors of the reaction $^{24}Mg(^{16}O,^{12}C)^{28}Si$ g.s., was obtained comparing the experimental differential cross-section of this reaction at forward angles with the DWUCK calculated transfer cross-section.

c) The normalized $\bar{V}_{pol}$ is added to the optical potential and the radial Schrödinger equation is solved, generating the exact, perturbed wave function in the elastic channel $\bar{\psi}^0_\ell(r)$. From this wave-function we calculated the perturbed scattering matrix $\bar{S}_{\ell,0}$, which is compared on Fig. 5 with the unperturbed

scattering matrix $S_{\ell,0}$. The slight difference between them is localized around the grazing angular momentum, as can be seen in the insert of Fig. 5, where the difference $|\bar{S}_{\ell,0} - S_{\ell,0}|$ is shown.

d) This exact wave-function is used in DWUCK to calculate the elastic angular distribution, the inelastic excitation cross-sections and the transfer cross-sections in ZR and NR approximation for all transfer processes, namely:

$$^{24}Mg(^{16}O,^{12}C)^{28}Si(0^+)$$

$$^{24}Mg(^{16}O,^{12}C)^{28}Si(2^+)$$

$$^{24}Mg(^{16}O,^{20}Ne)^{20}Ne$$

including the effect of $\bar{V}_{pol}$ in all these processes. The same code permitted us to calculate these cross-sections without including $\bar{V}_{pol}$, in order to compare both calculations.

2. Calculations of the cross-sections for the $^{24}Mg + ^{16}O$ system, including the polarization potential:

a) The reaction $^{24}Mg(^{16}O,^{12}C)^{28}Si$ g.s.

The differential transfer cross-sections were calculated without and in the presence of $\bar{V}_{pol}$ and normalized to experimental data at forward angles.

The effect of $\bar{V}_{pol}$ in the transfer angular

distribution is small at forward angles, but produces strong oscillations and rise in the backward angle region. However its effect in the backward angles is still smaller than the experimental cross-section. If we multiply $\bar{V}_{pol}$ by an additional factor of 1.9 the calculated transfer cross-section reproduces well the backward rise in the experimental data, as can be verified in Fig. 6, where we compare the complete experimental angular distribution of $^{24}Mg(^{16}O,^{12}C)^{28}Si$ g.s., including our data (open circles) and that of Paul[2] (full dots) with the calculated transfer cross-section in the presence of $\bar{V}_{pol}$ (continuous line) and without $\bar{V}_{pol}$ (dashed line). This additional normalization factor can be attributed to the off-shell effects, whose influence can modify the $\bar{V}_{pol}$ by a factor ranging from 1 to 4[7]. The reason to perform the final normalization of $\bar{V}_{pol}$ adjusting the backward cross-section of the $^{24}Mg(^{16}O,^{12}C)^{28}Si$ g.s. is that we assume that the backward anomaly in this channel is due exclusively to the dynamical α-transfer polarization potential $\bar{V}_{pol}$. In the calculations of other channels, this same normalization of $\bar{V}_{pol}$ will be maintained.

b) Elastic scattering $^{24}Mg(^{16}O,^{16}O)^{24}Mg$.

The $\bar{V}_{pol}$ is included in the Schrödinger equation, together with the optical potential ANL2. The elastic cross-section, calculated in the presence of these potentials, is

shown in Fig. 7 together with experimental data. The calculation provides the backward rise, which is somewhat overestimated. Many attempts were performed, using many different optical potentials, in order to reduce the effect in the elastic channel, without reducing in the α-transfer channel, but in no way we could change this behaviour. This fact can be an indication that the coupling to other channels (inelastic, α-pickup), which are neglected in this calculation, are more important in the elastic channel than in the α-stripping ground state transition.

c) Inelastic scattering $^{24}Mg(^{16}O, ^{16}O)^{24}Mg(2^+, 1.37\ MeV)$.

The inelastic cross-section was calculated by DWUCK, using collective nuclear form factors, given by the derivative of the optical potential:

$$F_N(r) = \delta_2^N \left(V \frac{df_R(r)}{dr} + \cdots \frac{df_I(r)}{dr} \right) \qquad (7)$$

where $\delta_2^N = \beta_2^N R_N$ is the nuclear deformation length and the nuclear optical potential is

$$U(r) = -V f_R(r) - iW f_I(r) \quad . \qquad (8)$$

The Coulomb form factor is:

$$F_C(r) = \frac{4\pi}{5} \frac{Ze\,[B(E2\uparrow)]^{\frac{1}{2}}}{r^3} = \frac{3}{5} \frac{Z^2 e^2 R_C^2 \beta_2^C}{r^3} \quad . \qquad (9)$$

Using $R_C = r_{0C} A_T^{1/3}$ with $r_{0C} = 1.495$ fm and the adopted value of $B(E2\uparrow) = 430\ e^2 fm^4$, we obtain $\beta_2^C = 0.3897$ and $\delta_2^C = \beta_2^C R_C = 1.68$. The nuclear deformation length $\delta_2^N = \beta_2^N R$, obtained in other inelastic scattering measurements on ^{24}Mg [10,11], is around 1.5 and 1.6. We also performed coupled-channels calculations with the code ECIS, where we obtained a good accord with our forward inelastic data, using the ANL2 potential, $\beta_2^C = 0.3897$ and $\beta_2^N R_N = 1.5$. However, when these deformation parameters are used in DWBA approximation the agreement is much worse. In order to get a good fit of the data using DWUCK, we have to increase β_2^C to 0.542 and reduce δ_2^N to 0.862. The full inelastic experimental angular distribution and the calculations with $\bar{V}_{pol}$ (continuous line) and without $\bar{V}_{pol}$ (dashed line) are shown in Fig. 8. The deformation parameters used in this calculation are: $\delta_2^N = 0.862$ and $\beta_2^C = 0.542$. The effect of $\bar{V}_{pol}$ is again small at forward angles, but produces an increase and strong oscillations at the backward angles. However the backward cross-section is still somewhat underestimated.

d) The reaction $^{24}Mg(^{16}O, ^{12}C)^{28}Si(2^+, 1.78\ MeV)$

The transfer cross-sections, calculated without and in the presence of $\bar{V}_{pol}$ and normalized to experimental data at forward angles, are shown in Fig. 9, together with experimental angular distribution. The calculation without $\bar{V}_{pol}$ (dashed

curve) reproduces well the forward angle cross-section but fails completely at backward angles. The effect of the inclusion of $\bar{V}_{pol}$ again is small at forward angles and produces oscillations and rise at backward angles, which are however underestimated.

e) The reaction $^{24}Mg(^{16}O,^{20}Ne)^{20}Ne$ g.s.

The outgoing particles are identical and this fact implies in two modifications in the calculation of the transfer cross-section[12], there is a double-counting in the detection, because the detector cannot distinguish between ^{20}Ne originating from target or projectile; and the outgoing wave-function has to be symmetrized. The transfer cross-section, calculated in these conditions, can be written as:

$$\frac{d\sigma}{d\Omega} = |f(\vartheta,\varphi) + f(\pi-\vartheta, \varphi+\pi)|^2$$

where $f(\vartheta,\varphi)$ is the transfer amplitude calculated without considering the identity of particles. Only even partial waves will contribute to the summed transfer amplitude and the cross-section will be symmetrical around 90°, with a maximum at 90°.

We have calculated the transfer cross-section without $\bar{V}_{pol}$, taking into account both effects affecting identical particles, and again normalizing the calculation to the mean behaviour of forward angle experimental data. The

calculation, presented on Fig. 10 as a dashed line, produces a maximum at 90^{o}, in desaccord with experimental result, and almost no oscillations at forward and backward angles, showing even a smooth bell shape, with maximum at $\theta_{gr} \sim 40^{o}$, due to negative Q-value of the reaction (- 4.58 MeV). The effect of inclusion of $\bar{V}_{pol}$ in the calculation is to introduce oscillations at forward and backward angles which agree well with experimental data. However, the maximum at 90^{o} remains even with $\bar{V}_{pol}$, indicating that the experimental minimum is not related to this α-transfer coupling.

Minimum at 90^{o} has also been observed in other cases of identical particle scattering, as the elastic scattering $^{12}C(^{12}C,^{12}C)^{12}C$ at some energies[13,14]. We are investigating the origin of the minimum observed in our reaction.

f) The reactions $^{24}Mg(^{16}O,^{20}Ne)^{20}Ne$ leading to excited states (2^{+} at 1.63 MeV and 4^{+} at 4.25 MeV) in ^{20}Ne

We performed calculations with PTOLEMY for these reactions and verified that the cross section for the reaction $^{24}Mg(^{16}O,^{20}Ne^{*})^{20}Ne$ g.s. is much higher than for the reaction $^{24}Mg(^{16}O,^{20}Ne)^{20}Ne^{*}$. The spectroscopic factors for $^{16}O + \alpha \rightarrow {}^{20}Ne^{*}$ are also higher than for $^{24}Mg - \alpha \rightarrow {}^{20}Ne^{*}$. As a consequence, the experimental angular distributions for the excitation of one ^{20}Ne to its 2^{+} or 4^{+} states respectively, can be considered essentially as projectile excitation reaction, as: $^{24}Mg(^{16}O,^{20}Ne(2^{+},1.63))^{20}Ne$ g.s.,

$^{24}Mg(^{16}O,^{20}Ne(4^+,4.25))^{20}Ne$ g.s.. In DWUCK the projectile excitation cannot be taken into account and for these reason, we cannot calculate at the preset stage, the effect of $\ddot{V}_{pol}$ on the reactions leading to excited states of ^{20}Ne.

g) Spectroscopic informations

In order to show, that our results are quantitatively consistent, we compared our relative normalization N (defined as the normalization factor of the transition considered (determined at forward angles), divided by the normalization factor of the α-stripping ground state transition), with the ratio of the theoretical spectroscopic factors corresponding to these transitions. In Table II we show the theoretical α-spectroscopic factors S_1 and S_2, for the target and projectile nuclei involved in these reactions[15,16], normalized relative to the $^{20}Ne_{gs} \rightarrow {}^{16}O_{gs} + \alpha$ spectroscopic factor. The spectroscopic factors of the reactions are also presented in the third column of Table II as products of target and projectile spectroscopic factors. In the fourth column we show the relative spectroscopic factors of these reactions, normalized to the ground state transition of the $(^{16}O,^{12}C)$ reaction. In the fifth column we show our relative normalization factors N, which are in excellent agreement with the relative theoretical spectroscopic factors of these reactions.

IV. CONCLUSIONS

We have calculated the dynamic α-transfer polarization potential $\bar{V}_{pol}$ and introduced into our elastic, inelastic and transfer calculations in order to estimate its effect on the back-angle anomalies observed in many channels of the $^{24}Mg + ^{16}O$ system. The coupling between the elastic and α-stripping channel explains in a fairly quantitative way the anomalies observed, overestimating the effect in the elastic channel and somewhat underestimating in some other channels. This fact can be an indication that other channel couplings can also be important and should be taken into account.

ACKNOWLEDGMENTS

We would like to thank Prof. M.S. Hussein and Prof. L.C. Gomes for very fruitful discussions.

REFERENCES

1) G.K. Gelbke, T. Awes, U.E.P. Berg, J. Barrette, M.J. Levine and P. Braun-Munzinger, Phys. Rev. Lett. 41, 1778 (1978).

2) M. Paul, S.J. Sanders, D.P. Geesaman, W. Henning, D.G. Kovar, C. Olmer, J.P. Schiffer, J. Barrette and M.J. Levine, Phys. Rev. C21, 1802 (1980).

3) R. Lichtenthaler Jr., A. Lépine-Szily, A.C.C. Villari, W. Mittig, V.J.G. Porto and C.V. Acquadro, Phys. Rev. C26, 2487 (1982).

4) W.E. Frahn and M.S. Hussein, Nucl. Phys. A346, 237 (1980).

5) L.F. Canto, R. Donangelo, M.S. Hussein and A. Lépine-Szily, Phys. Rev. Lett. 51, 95 (1983).

6) M.S. Hussein, A.N. Aleixo, L.F. Canto, P. Carrilho, R. Donangelo and L.S. de Paula, J. Phys. G 13, 967 (1987).

7) T. Udagawa, K.S. Low and T. Tamura, Phys. Rev. C28, 1033 (1983).

8) M.H. Macfarlane and S.C. Pieper, Argonne National Laboratory Report ANL76-11, unpublished.

9) S.L. Tabor, D.F. Geesaman, W. Henning, D.G. Kovar, K.E. Rehm and F.W. Prosser Jr., Phys. Rev. C17, 2136 (1978).

10) W. Mittig, P. Charles, S.M. Lee, I. Badawy, B. Berthier, B. Fernandez and J. Gastebois, Nucl. Phys. A233, 48 (1974).

11) J.S. Eck, D.O. Elliott and W.J. Thompson, Phys. Rev. C16, 1020 (1977).

12) A. Messiah, Mécanique Quantique, Dunod, Paris, 1960, Tome II, p. 514.

13) W. Reilly, R. Wieland, A. Gobbi, M.W. Saks, J. Maher, R.H. Siemssen, D. Mingay and D.A. Bromley, Nuovo Cim. 13A, 913 (1973).

14) R.M. Wieland, R.G. Stokstad, G.R. Satchler and L.D. Rickertsen, Phys. Rev. Lett. 37, 1458 (1976).

15) K.T. Hecht and D. Braunschweig, Nucl. Phys. A244, 365 (1975) and J.P. Draayer, Nucl. Phys. A237, 157 (1975).

16) C. Detraz, H.H. Duhm and H. Hafner, Nucl. Phys. A[illegible], 488 (1970).

FIGURE CAPTIONS

Fig. 1 - Angular distributions of the $^{24}Mg(^{16}O,^{16}O)^{24}Mg$ elastic scattering and $^{24}Mg(^{16}O,^{16}O)^{24}Mg(2^+, 1.37\ MeV)$ inelastic scattering.

Fig. 2 - Angular distributions of the $^{24}Mg(^{16}O,^{12}C)^{28}Si(0^+,g.s.)$ and $^{24}Mg(^{16}O,^{12}C)^{28}Si(2^+, 1.78\ MeV)$ reactions.

Fig. 3 - Angular distributions of the $^{24}Mg(^{16}O,^{20}Ne)^{20}Ne(0^+,g.s.)$, $^{24}Mg(^{16}O,^{20}Ne)^{20}Ne(2^+,1,63\ MeV)$, $^{24}Mg(^{16}O,^{20}Ne(2^+,1.63\ MeV)^{20}Ne(2^+$ 1.63 MeV) and $^{24}Mg(^{16}O,^{20}Ne)^{20}Ne(4^+,4.25\ MeV)$ reactions.

Fig. 4 - Full experimental angular distribution of the $^{24}Mg(^{16}O,^{12}C)^{28}Si(0^+,g.s.)$ reaction, our data are indicated by open circles and data of Paul et al.[2] with full dots. The continuous line is the cross-section calculated by PTOLEMY and the dashed line is the calculation by DWUCK, using the potential ANL2 in both channels. The calculations are normalized to experimental data at forward angles.

Fig. 5 - The full line indicates the modulus of the perturbed scattering matrix $|S_{\ell,0}|$ and the dashed line of the unperturbed scattering matrix $|S_{\ell,0}|$, the insert indicates the modulus of the difference $|S_{\ell,0} - S_{\ell,0}|$.

TABLE CAPTIONS

Table I - Optical potential parameters.

Table II - Comparison of relative theoretical spectroscopic factors of the reactions $^{24}Mg(^{16}O,^{12}C)^{28}Si$ and $^{24}Mg(^{16}O,^{20}Ne)^{20}Ne$ with our relative normalization factors N, defined in text. S_1 refers to target spectroscopic factors and S_2 to projectile spectroscopic factors, S_1S_2 refers to the reactions indicated and $S_1S_2/S_1S_2(^{16}O,^{12}C)_{gs}$ are the reaction spectroscopic factors normalized to the ground state transition of the $(^{16}O,^{12}C)$ reaction. N are our relative normalization factors.

Footnote to table II

The theoretical spectroscopic factors S_1 and S_2 were normalized such that $S_\alpha = 1$ for $^{16}O_{gs} + \alpha \rightarrow {}^{20}Ne_{gs}$.

a) ref. 15.

b) calculations of H. Yoshida, quoted in ref. 16 .

TABLE I

Potential	V (MeV)	v_r (fm)	a_r (fm)	W (MeV)	v_I (fm)	a_I (fm)
ANL2	10.0	1.452	0.345	23.0	1.272	0.376

Fig. 6 - Experimental angular distribution of $^{24}Mg(^{16}O,^{12}C)^{28}Si(0^+,g.s.)$ reaction, our data are the open circles and the data of Paul[2] the full dots. The continuous line is the cross-section calculated in the presence of $\bar{V}_{pol}$ and the dashed line without $\bar{V}_{pol}$.

Fig. 7 - Experimental angular distribution of $^{24}Mg(^{16}O,^{16}O)^{24}Mg$ elastic scattering, our data are the open circles and the data of Paul[2] are the full dots. The continuous line is the cross-section calculated in the presence of $\bar{V}_{pol}$ and the dashed line without $\bar{V}_{pol}$.

Fig. 8 - Experimental angular distribution of $^{24}Mg(^{16}O,^{16}O)^{24}Mg(2^+,1.37\ MeV)$ inelastic scattering, our data are the open circles and the data of Paul[2] are the full dots. The continuous line is the cross-section calculated in the presence of $\bar{V}_{pol}$ and the dashed line without $\bar{V}_{pol}$.

Fig. 9 - Experimental angular distribution of $^{24}Mg(^{16}O,^{12}C)^{28}Si(2^+,1.78\ MeV)$ reaction, our data are the open circles and the data of Paul[2] are the full dots. The continuous line is the cross-section calculated in the presence of $\bar{V}_{pol}$ and the dashed line without $\bar{V}_{pol}$.

Fig. 10 - Experimental angular distribution of $^{24}Mg(^{16}O,^{20}Ne)^{20}Ne(0^+,g.s.)$ reaction. The continuous line is the cross-section calculated in the presence of $\bar{V}_{pol}$ and the dashed line without $\bar{V}_{pol}$.

TABLE II

$S_1(^{24}Mg + \alpha \rightarrow {}^{28}Si\ (J^\pi))$		$S_2(^{12}C + \alpha \rightarrow {}^{16}O)$	S_1S_2	$\frac{S_1S_2}{S_1S_2(^{16}O, {}^{12}C)_{gs}}$	N
J^π					
0^+	0.41[a]	1.62[b]	0.664	1	1
2^+	0.094[a]	1.62[b]	0.152	0.23	0.23
$S_1(^{24}Mg - \alpha \rightarrow {}^{20}Ne(J^\pi))$		$S_2(^{16}O + \alpha \rightarrow {}^{20}Ne)$			
J^π					
0^+	0.35[a]	1.0	0.35	0.53	0.52

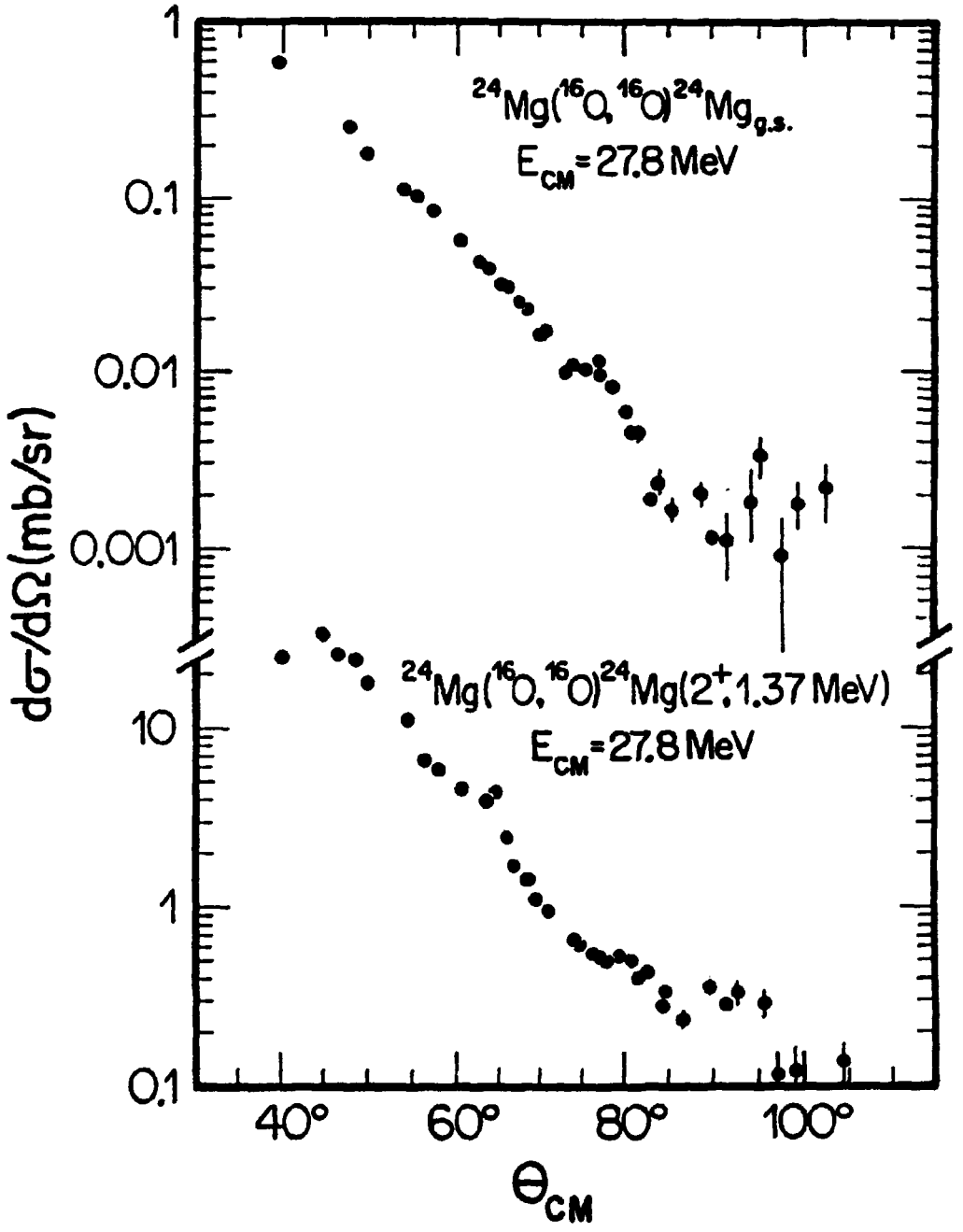
1
0.1
0.01
0.001
10
1
0.1
dσ/dΩ(mb/sr)
$^{24}Mg(^{16}O,^{16}O)^{24}Mg_{g.s.}$
E_{CM}=27.8 MeV
$^{24}Mg(^{16}O,^{16}O)^{24}Mg(2^+,1.37\,MeV)$
E_{CM}=27.8 MeV
40°
60°
80°
100°
Θ_{CM}

Fig 1

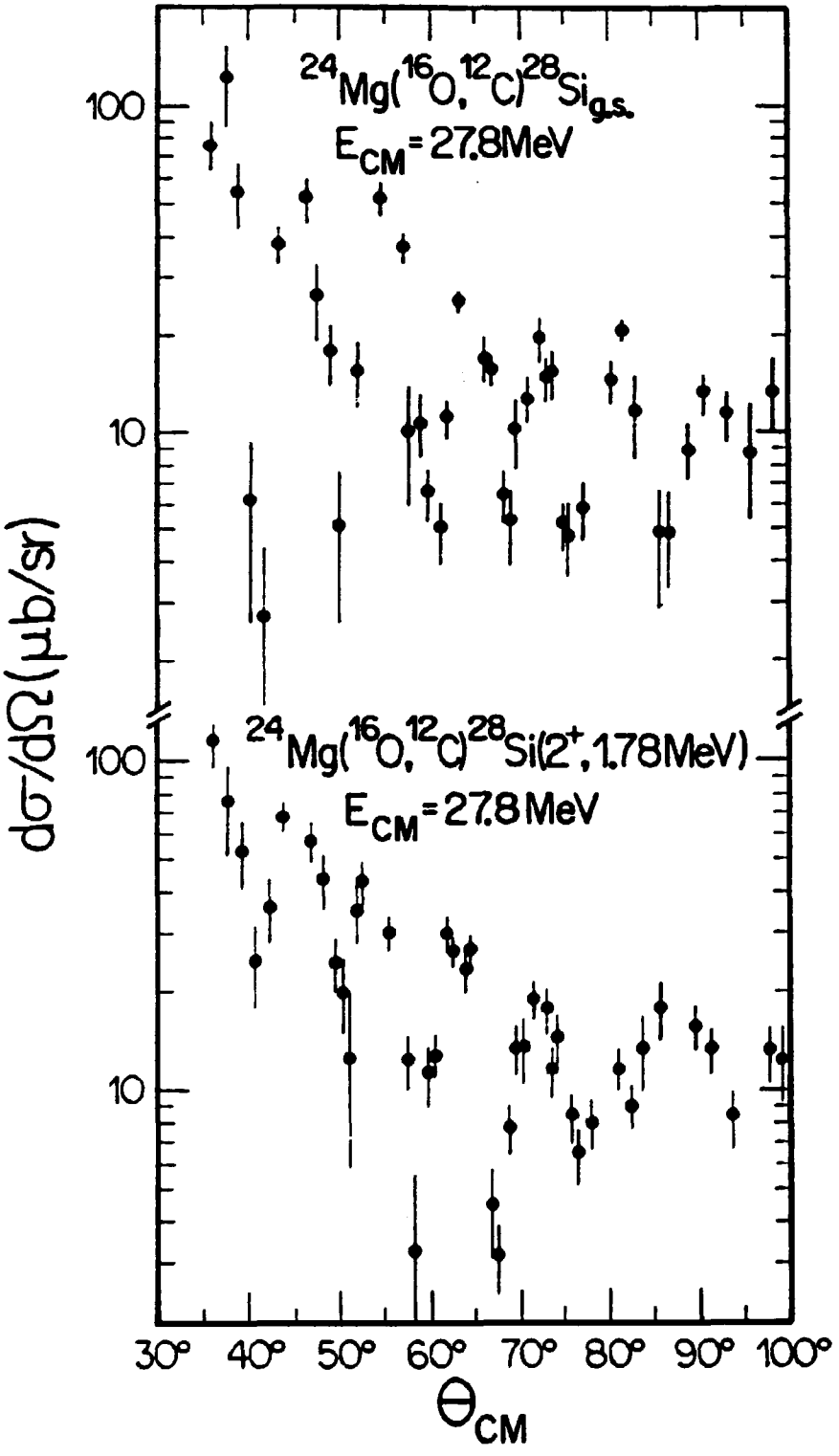
$^{24}Mg(^{16}O,^{12}C)^{28}Si_{g.s.}$
E_{CM}=27.8MeV
$^{24}Mg(^{16}O,^{12}C)^{28}Si(2^+,1.78MeV)$
E_{CM}=27.8MeV
100
10
100
10
$d\sigma/d\Omega(\mu b/sr)$
30° 40° 50° 60° 70° 80° 90° 100°
Θ_{CM}

Fig. 2

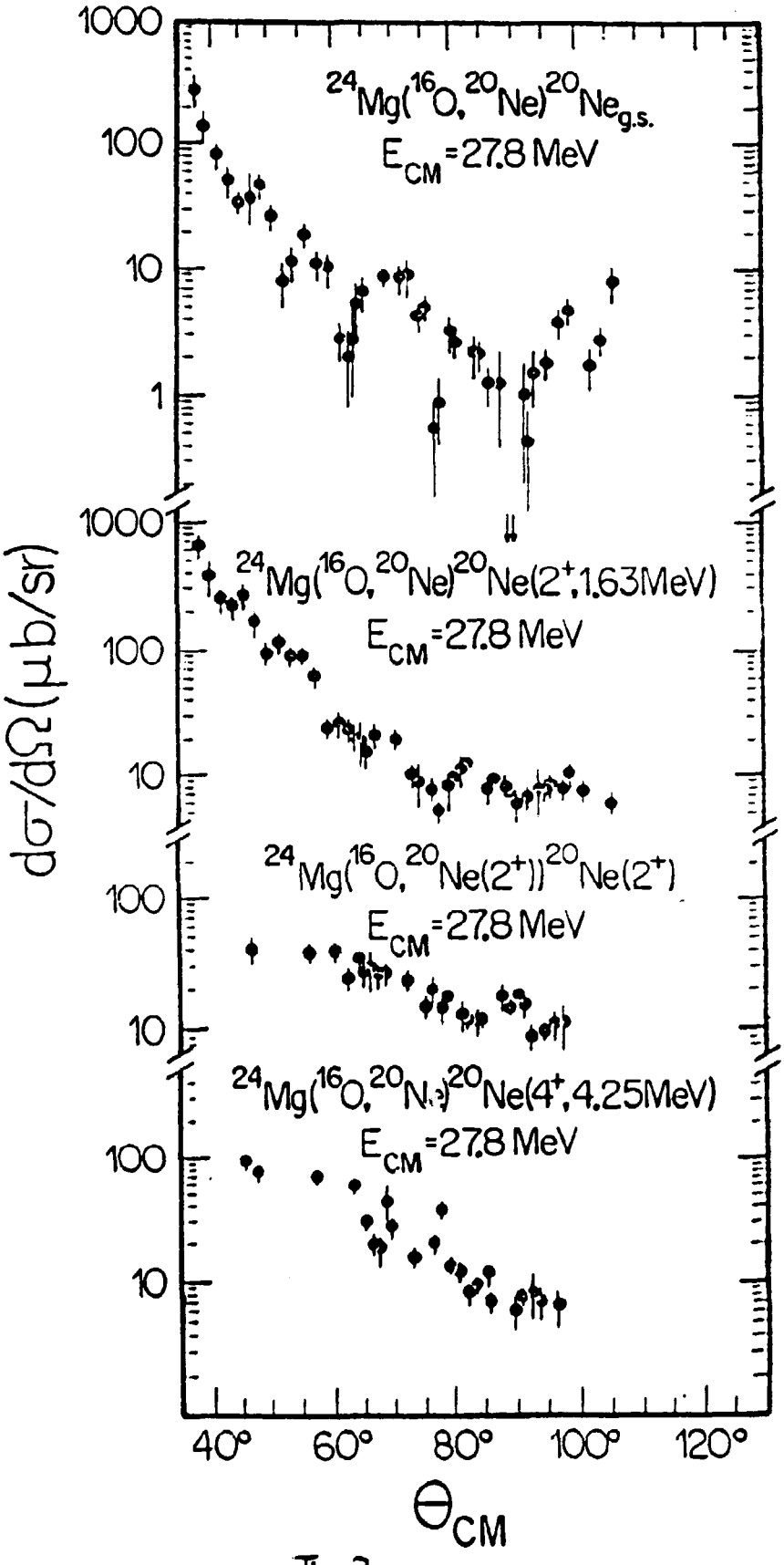
$^{24}Mg(^{16}O,^{20}Ne)^{20}Ne_{g.s.}$
E_{CM}=27.8 MeV
$^{24}Mg(^{16}O,^{20}Ne)^{20}Ne(2^+,1.63MeV)$
E_{CM}=27.8 MeV
$^{24}Mg(^{16}O,^{20}Ne(2^+))^{20}Ne(2^+)$
E_{CM}=27.8 MeV
$^{24}Mg(^{16}O,^{20}Ne)^{20}Ne(4^+,4.25MeV)$
E_{CM}=27.8 MeV
$d\sigma/d\Omega(\mu b/sr)$
1000
100
10
1
40°
60°
80°
100°
120°
Θ_{CM}

Fig. 3

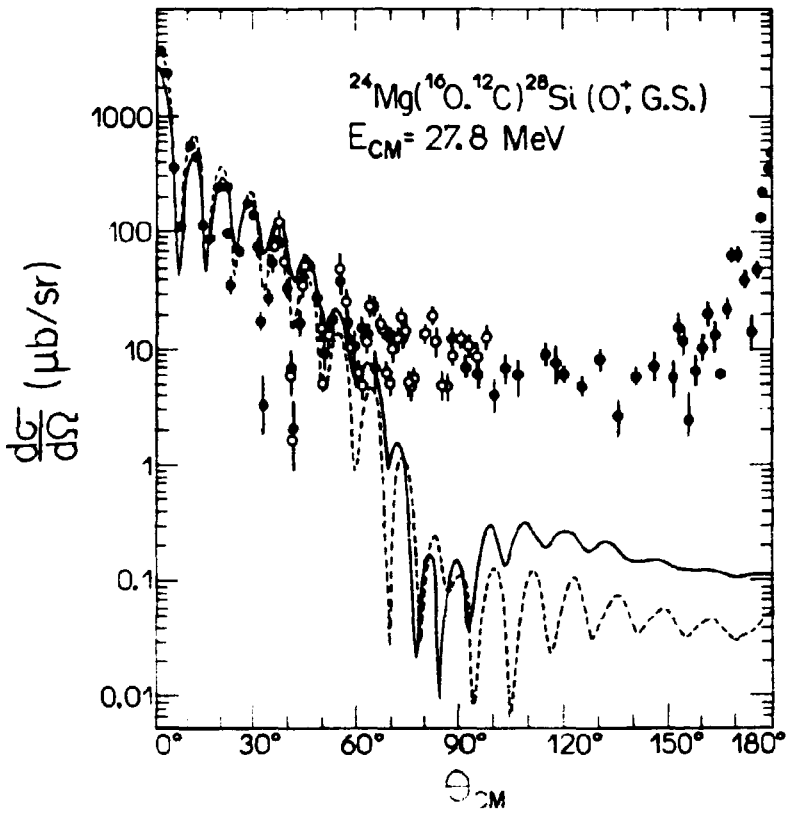
$^{24}Mg(^{16}O,^{12}C)^{28}Si$ (0^+, G.S.)
E_{CM}= 27.8 MeV
1000
100
10
1
0.1
0.01
0°
30°
60°
90°
120°
150°
180°
θ_{CM}
$\frac{d\sigma}{d\Omega}$ (μb/sr)

fig 4

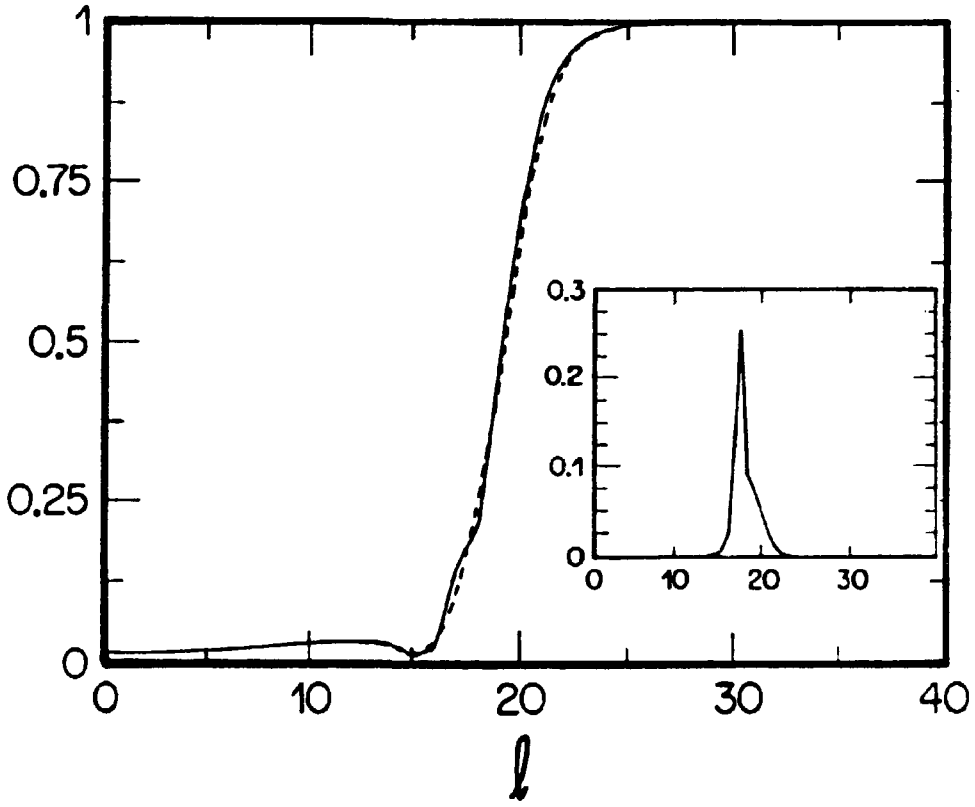

Fig. 5

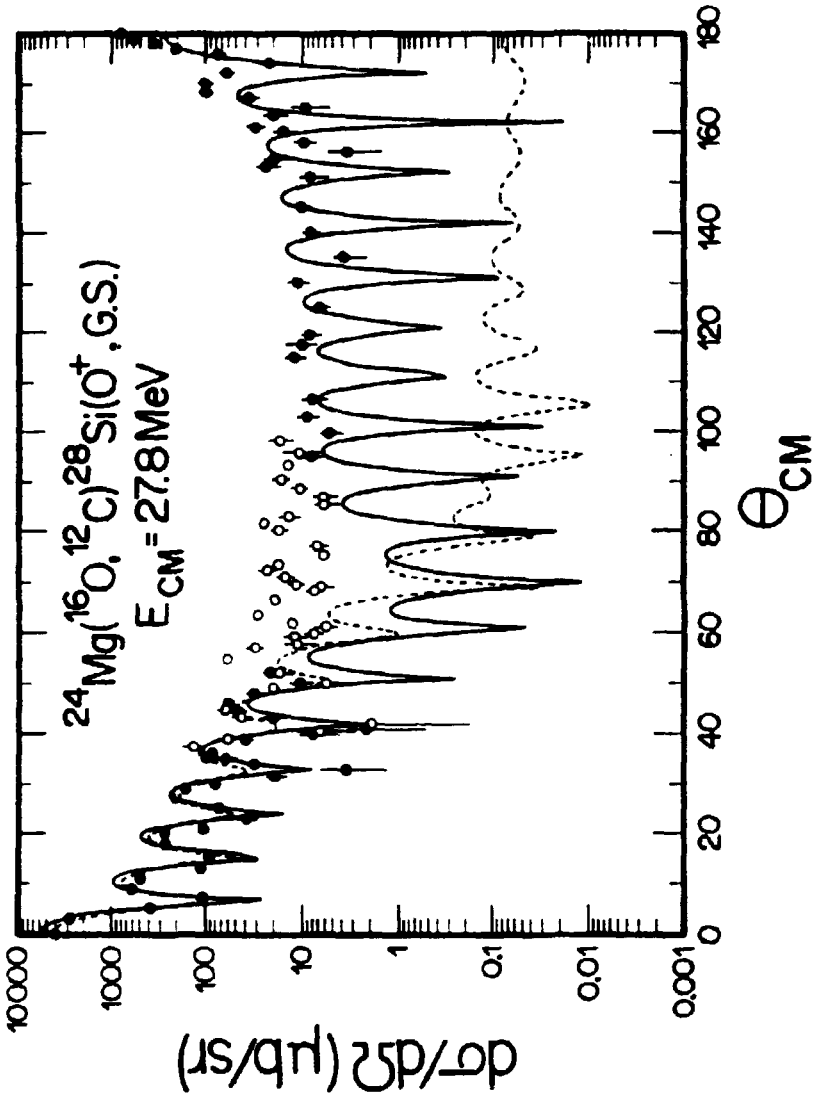
$^{24}Mg(^{16}O,^{12}C)^{28}Si(0^+,G.S.)$
E_{CM}= 27.8MeV
dσ/dΩ (μb/sr)
θ_{CM}
10000
1000
100
10
1
0.1
0.01
0.001
0
20
40
60
80
100
120
140
160
180

Fig 6

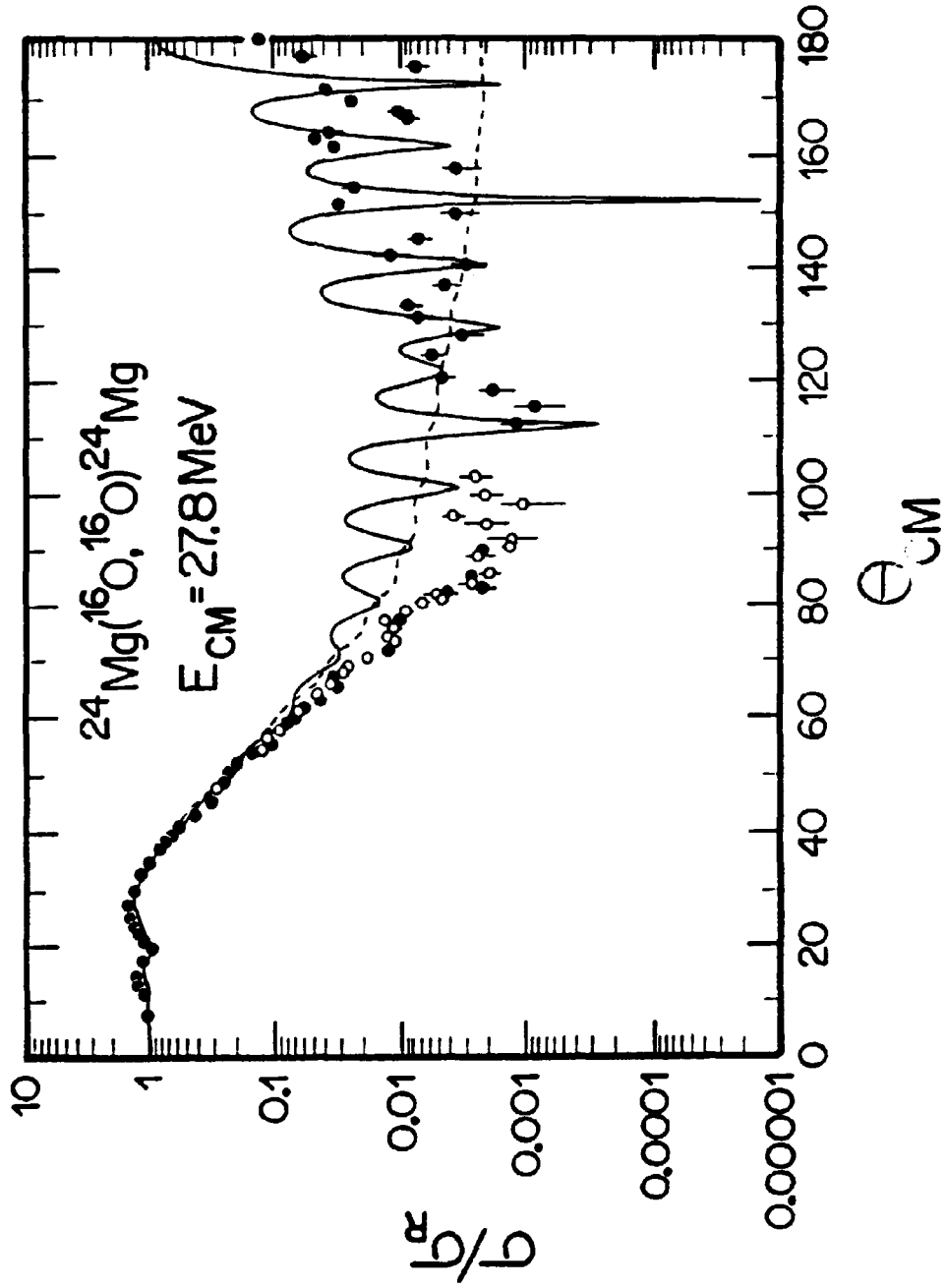
$^{24}Mg(^{16}O,^{16}O)^{24}Mg$
$E_{CM}=27.8MeV$
σ/σ_R
Θ_{CM}
10
1
0.1
0.01
0.001
0.0001
0.00001
0
20
40
60
80
100
120
140
160
180

Fig. 7

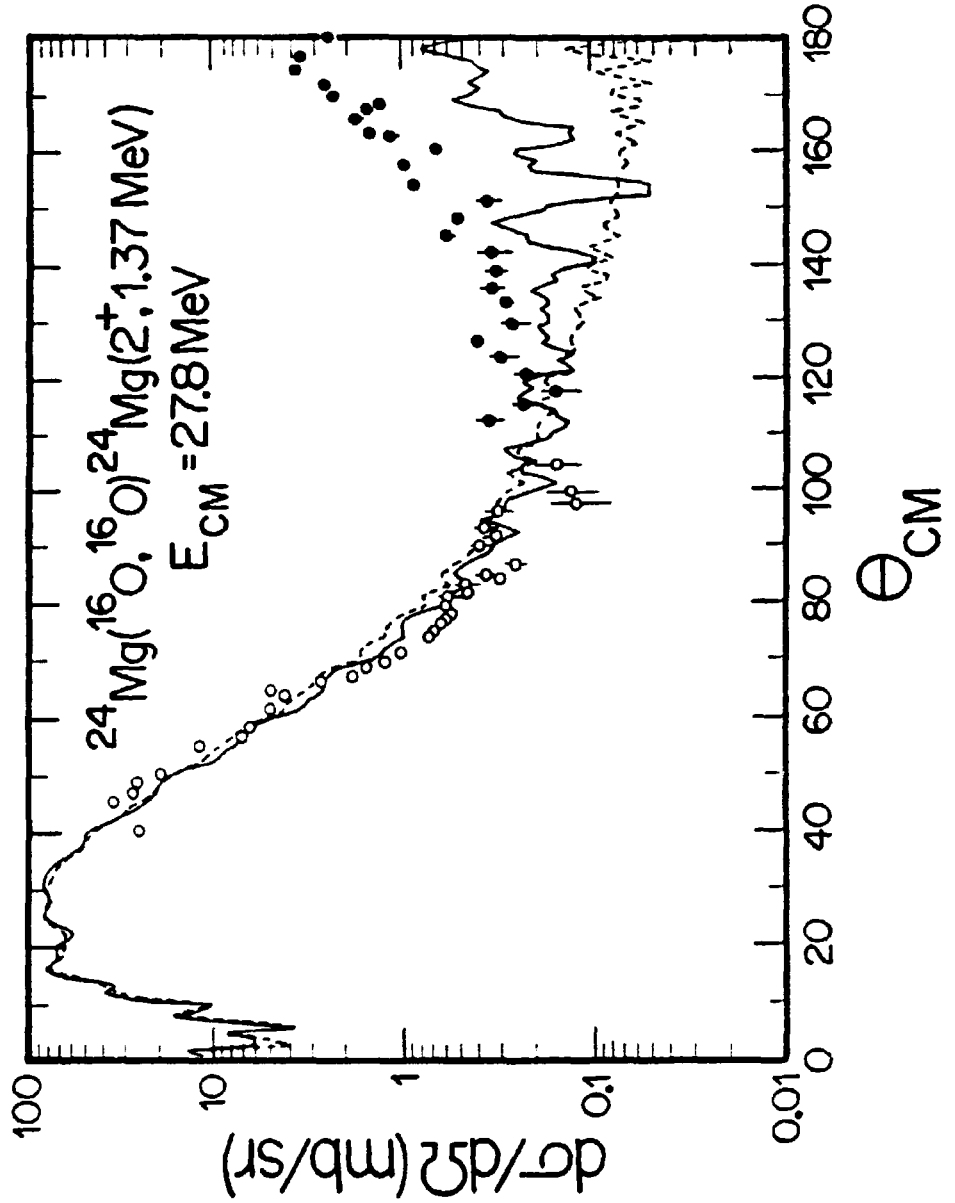
$^{24}Mg(^{16}O,^{16}O)^{24}Mg(2^+,1.37\,MeV)$
$E_{CM}=27.8\,MeV$
dσ/dΩ (mb/sr)
100
10
1
0.1
0.01
0
20
40
60
80
100
120
140
160
180
Θ_{CM}

Fig. 8

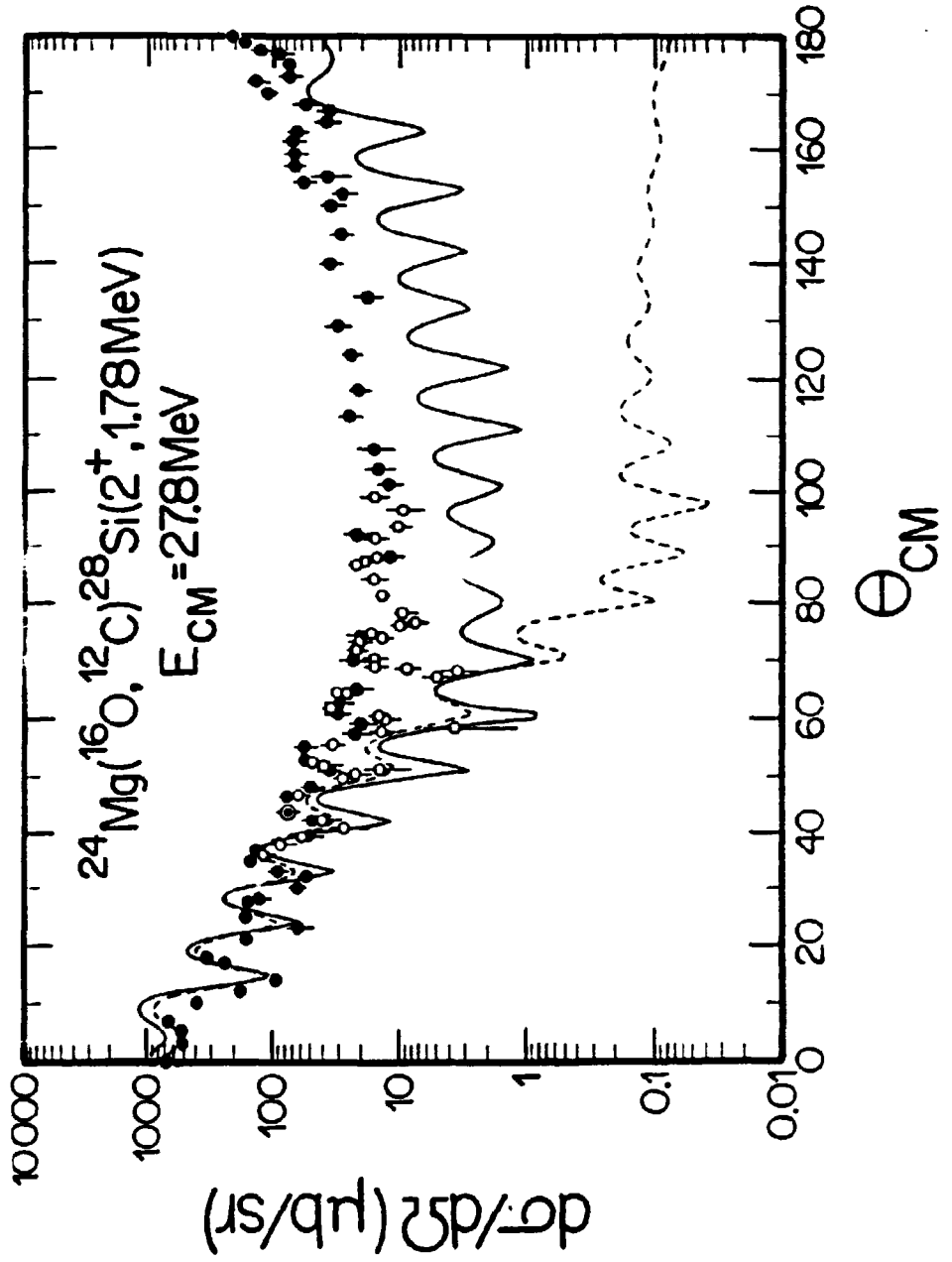
$^{24}Mg(^{16}O,^{12}C)^{28}Si(2^+,1.78MeV)$
$E_{CM}=27.8MeV$
$d\sigma/d\Omega$ (μb/sr)
θ_{CM}
10000
1000
100
10
1
0.1
0.01
0
20
40
60
80
100
120
140
160
180

Fig. 9